The crystal and magnetic structure of Li-aegirine LiFe3+Si2O6: A temperature-dependent study

Article *in* Physics and Chemistry of Minerals · June 2001

DOI: 10.1007/s002690100159

CITATIONS
65

READS
131

8 authors, including:

Günther J Redhammer
University of Salzburg
288 PUBLICATIONS **2,451** CITATIONS

SEE PROFILE

Georg Amthauer
University of Salzburg
513 PUBLICATIONS **3,380** CITATIONS

SEE PROFILE

Brigitte Bitschnau
Graz University of Technology
57 PUBLICATIONS **814** CITATIONS

SEE PROFILE

Phys Chem Minerals (2001) 28: 337–346

ORIGINAL PAPER

G. J. Redhammer · G. Roth · W. Paulus · G. André
W. Lottermoser · G. Amthauer · W. Treutmann
B. Koppelhuber-Bitschnau

The crystal and magnetic structure of Li-aegirine $LiFe^{3+}Si_2O_6$: a temperature-dependent study

Received: 14 April 2000 / Accepted: 29 January 2001

Abstract Single crystals of Li-aegirine $LiFe^{3+}Si_2O_6$ were synthesized at 1573 K and 3 GPa, and a polycrystalline sample suitable for neutron diffraction was produced by ceramic sintering at 1223 K. $LiFe^{3+}Si_2O_6$ is monoclinic, space group $C2/c$, $a = 9.6641(2)$ Å, $b = 8.6612(3)$ Å, $c = 5.2924(2)$ Å, $\beta = 110.12(1)^\circ$ at 300 K as refined from powder neutron data. At 229 K Li-aegirine undergoes a phase transition from $C2/c$ to $P2_1/c$. This is indicated by strong discontinuities in the temperature variation of the lattice parameters, especially for the monoclinic angle β and by the appearance of Bragg reflections (hkl) with $h + k \neq 2n$. In the low-temperature form two non-equivalent Si-sites with $\langle SiA–O\rangle = 1.622$ Å and $\langle SiB–O\rangle = 1.624$ Å at 100 K are present. The bridging angles of the SiO_4 tetrahedra O3–O3–O3 are 192.55(8)° and 160.02(9)° at 100 K in the two independent tetrahedral chains in space group $P2_1/c$, whereas it is 180.83(9)° at 300 K in the high-temperature $C2/c$ phase, i.e. the chains are nearly fully expanded. Upon the phase transition the Li-coordination changes from six to five. At 100 K four Li–O bond lengths lie within 2.072(4)–2.172(3) Å, the fifth Li–O bond length is 2.356(4) Å, whereas the Li–O3 A bond lengths amount to 2.796(4) Å. From ^{57}Fe Mössbauer spectroscopic measurements between 80 and 500 K the structural phase transition is characterized by a small discontinuity of the quadrupole splitting. Temperature-dependent neutron powder diffraction experiments show first occurrence of magnetic reflections at 16.5 K in good agreement with the point of inflection in the temperature-dependent magnetization of $LiFe^{3+}Si_2O_6$. Distinct preordering phenomena can be observed up to 35 K. At the magnetic phase transition the unit cell parameters exhibit a pronounced magneto-striction of the lattice. Below T_N Li-aegirine shows a collinear antiferromagnetic structure. From our neutron powder diffraction experiments we extract a collinear antiferromagnetic spin arrangement within the a–c plane.

Key words Li-aegirine · Clinopyroxene · Diffraction · Phase transition · Magnetism

G. J. Redhammer (✉) · G. Roth
Institut für Kristallographie,
Rheinisch Westfälische Technische Hochschule Aachen,
Jägerstraße 17/19, 54056 Aachen, Germany
e-mail: guenther.redhammer@sbg.ac.at

W. Paulus · G. André
Laboratoire Léon Brillouin, CEA Saclay,
91191 Gif-Sur-Yvette Cedex, France

W. Lottermoser · G. Amthauer
Institut für Mineralogie, Universität Salzburg,
Hellbrunnerstraße 34, 5020 Salzburg, Austria

W. Treutmann
Institut für Mineralogie, Philipps Universität Marburg,
Hans-Meerweinstraße, 35032 Marburg/Lahn, Germany

B. Koppelhuber-Bitschnau
Institut für Physikalische Chemie,
Erzherzog Johann Universität Graz,
Technikerstraße, 8010 Graz, Austria

Introduction

Li-aegirine $LiFe^{3+}Si_2O_6$ is the homologue to the naturally occurring mineral spodumene $LiAlSi_2O_6$. Both compounds belong to the clinopyroxene group and crystallize in space group $C2/c$ at 300 K. The room temperature structure was first determined by Clark et al. (1969). The crystallographic details of the $C2/c$ clinopyroxene structure are reported herein. Behruzi et al. (1984) proposed a phase transition to $P2_1/c$ at 228 K for $LiFe^{3+}Si_2O_6$ but gave no details on the crystal structure except for a note on the change of the Li-coordination from six to five in the low-temperature form. Two kinds of silicate chains arise in the low-temperature phase, which are kinked by different angles smaller than 180°.

Magnetic susceptibility measurements on Li-aegirine single crystals by Baum et al. (1988) revealed a distinct magnetic transition to a collinear antiferromagnetic structure with the c-axis as the easy direction of the

magnetization at $T_N = 19.5(5)$ K. Lottermoser et al. (1998) performed single-crystal Mössbauer and neutron powder diffraction measurements but could not find clear evidence for the $C2/c \rightarrow P2_1/c$ phase transition on the basis of neutron powder diffraction data, recorded at 35 K. A refinement of the 35 K neutron powder diffraction data in $C2/c$ was problematic; however, a reduction to $P2_1/c$ reduced R values significantly. Surprisingly, no additional reflections characteristic for $P2_1/c$ could be observed. The Mössbauer experiments showed magnetic ordering at around 19 K in close agreement with the value reported by Baum et al. (1988). The single-crystal Mössbauer experiments yield a slight temperature-dependent angle of $\approx 42°$ between the main component of the electric field gradient, V_{zz}, and the b-axis. The internal magnetic field $H(0)$ was found to be mainly aligned parallel to the c-axis in agreement with the susceptibility measurements (Baum et al. 1988). A collinear spin arrangement within the a–c plane was also proposed by Lottermoser et al. (1998).

The aim of this study was to verify the presence or absence of a $C2/c \rightarrow P2_1/c$ phase transition. In order to achieve better precision, single crystals of high quality were used for X-ray diffraction experiments between 80 and 300 K. In addition, temperature-dependent powder X-ray diffraction experiments between 20 and 1023 K were performed to obtain a more complete picture on the thermal behavior of the Li-aegirine structure. On the basis of the results of single-crystal structure refinement, magnetization measurements, and powder neutron diffraction data, the magnetic structure of $LiFe^{3+}Si_2O_6$ was determined.

Experimental

Synthesis

Large amounts of $LiFe^{3+}Si_2O_6$, suitable for neutron powder diffraction experiments, were synthesized by solid-state ceramic sintering techniques at 1223 K and ambient pressure from stoichiometric mixtures of Li_2CO_3, Fe_2O_3, and SiO_2 in platinum crucibles. Well-crystallized Li-aegirine was obtained after several cycles of regrinding and rerunning the sintering product at the given temperature. The product was yellowish green and contained very small amounts of dilithium-disilicate $Li_2Si_2O_5$ as an impurity phase. Single crystals of $LiFeSi_2O_6$ were synthesized at 1573 K and 3 GPa in a piston cylinder apparatus. Synthetic Li-aegirine powder, produced as described above, was filled into small platinum tubes, which, in turn, were placed into an in-house-designed graphite–pyrophyllite furnace. This synthesis technique resulted in greenish, short prismatic single crystals up to 100 μ in size. Some experiments to grow single crystals of $LiFeSi_2O_6$ by flux techniques were also conducted using an Li_2MoO_4 flux and a sample to flux ratio of 1:10, yielding needle-like crystals up to 20 mm in length.

Structure refinement

Independently of the crystal growth techniques, all tested crystals showed more or less intense polysynthetic (micro)-twinning. The twinning is within the a–c plane, the b axis is common for the two twinning individua, and follows the Schwalbenschwanz law. Best-suited single crystals from the high-pressure experiments were used for subsequent structure refinement. Single-crystal X-ray diffraction data were collected on an image plate diffractometer (STOE-IPDS, MoKα radiation, pyrolytic graphite monochromator). The diffractometer was equipped with a cryostream liquid N2-cryostate (90–300 K, accuracy 0.1 K). The programs X-SHAPE (Stoe & Cie 1996) for numerical absorption correction and SHELXL (Sheldrick 1993) for structure refinement were employed. A total of 19 single-crystal datasets have been collected[1]. In the $P2_1/c$ low-temperature form, the atomic displacement parameters of iron and silicon atoms were refined only isotropically as they were not positively definite in the anisotropic form, most probably due to the pronounced pseudosymmetry (pseudo C-centering) in the low-temperature structure.

Neutron powder diffraction experiments were performed at the ORPHEE reactor (Laboratoire Léon Brilloin, CE Saclay, France) at 298 and 35 K on the 3T2 high-resolution powder diffractometer ($\lambda = 1.2268$ Å). Details and results for these measurements are given in Lottermoser et al. (1998). For the purpose of magnetic structure refinement, scattering experiments were also carried out on the G41 diffractometer ($\lambda = 2.4249$ Å) in a temperature range of $1.4 \leq T \leq 50$ K, 2Θ range of $5° \leq 2\Theta \leq 88°$, stepwidth 0.1°.

To obtain detailed information on the temperature variation of the lattice parameters, step-scan X-ray powder diffraction measurements were carried out in the temperature range 20–1023 K. The high-temperature measurements ($T > 300$ K) were recorded on a Θ–Θ Philips X'Pert diffractometer system, equipped with a PAAR HTK-16 high-temperature chamber, and operated with a copper X-ray tube. The low-temperature powder measurements ($T < 300$ K) were performed on a Philips X'Pert system equipped with a PAAR He-TTK low-temperature chamber.

The Rietveld refinements (Rietveld 1969) of the X-ray and neutron powder diffraction profiles were performed with FULLPROF (Rodriguez-Carajal 1996). The pseudo-Voigt function was used to simulate the peak shape; intensities within 12 times the peak full width at half maximum (FWHM) were assumed to contribute to one Bragg reflection. The angular dependence of peak FWHM was refined with the three parameters U, V, and W, using the formula of Cagliotti et al. (1958). Initial structure parameters were taken from the single-crystal structure refinements.

Mössbauer spectroscopy

Transmission ^{57}Fe Mössbauer experiments were carried out on a conventional Mössbauer apparatus (HALDER Electronic GmbH, Germany) using a ^{57}Co/Rh matrix single-line thin source, initial activity 50 mCi. The spectrometer was operated in constant acceleration mode with a symmetric triangular velocity shape and a multichannel analyzer with 1024 channels. The velocity range was ± 4 mm s^{-1} calibrated to α-iron . The isomer shift values thus are reported relative to α-iron. More details on Mössbauer spectroscopic measurements can be found in Lottermoser et al. (1998).

Results

Lattice parameters

Figure 1a–e displays the evolution of lattice parameters, extracted from powder X-ray diffraction experiments, as a function of temperature. In Table 1, the lattice parameters for selected temperatures are compiled. For temperatures $T > 300$ K, a, b, and c and the unit-cell volume follow a positive and linear correlation with

[1] The complete set of structural data (lattice parameters, atomic coordinations, bond lengths) is available from the corresponding author upon request. Data will also be deposited with the ICSD crystallographic database.

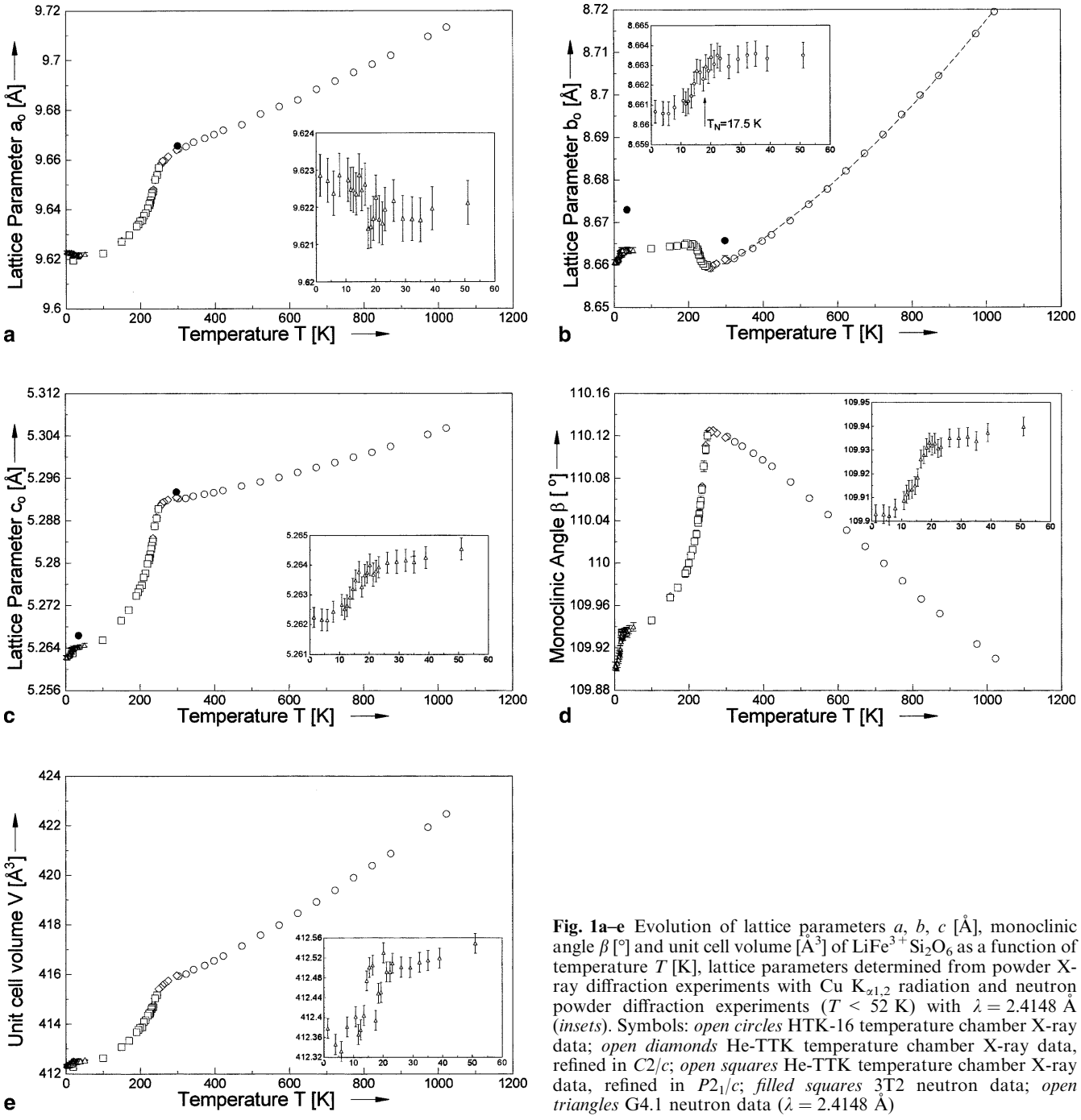

Fig. 1a–e Evolution of lattice parameters *a*, *b*, *c* [Å], monoclinic angle β [°] and unit cell volume [Å^3] of $LiFe^{3+}Si_2O_6$ as a function of temperature *T* [K], lattice parameters determined from powder X-ray diffraction experiments with Cu $K_{\alpha 1,2}$ radiation and neutron powder diffraction experiments ($T < 52$ K) with $\lambda = 2.4148$ Å (*insets*). Symbols: *open circles* HTK-16 temperature chamber X-ray data; *open diamonds* He-TTK temperature chamber X-ray data, refined in *C*2/*c*; *open squares* He-TTK temperature chamber X-ray data, refined in $P2_1/c$; *filled squares* 3T2 neutron data; *open triangles* G4.1 neutron data ($\lambda = 2.4148$ Å)

temperature, the monoclinic angle β decreases distinctly and more or less linearly with increasing *T*. Sharp discontinuities were, however, observed upon cooling at ≈ 245 K. Below this kink the decrease in *a* and *c* cell parameters with decreasing temperature is larger than above 245 K, while *b* increases between 245 and 210 K by 0.006 Å, but afterwards decreases again upon further cooling. The monoclinic angle β decreases with decreasing temperature below a very marked kink at ≈ 245 K. The lattice parameters determined in the single-crystal experiments show very similar behavior. At temperatures $T < 25$ K there are additional discontinuities, especially for the *b* and *c* cell parameters and for the monoclinic angle. These low-temperature unit-cell parameters were extracted from the refinement of the G4.1 powder neutron diffraction data and are displayed as insets at an enlarged scale for the temperature range 1.4–51.2 K in Fig. 1a–e.

Structure refinement

Details on the single-crystal structure refinements for three selected temperatures are given in Table 2. Atomic

Table 1 Lattice parameters of $LiFe^{3+}Si_2O_6$ at selected temperatures as determined from powder X-ray diffraction data. Estimated standard deviations (E.S.D's) are 0.0008 Å for *a*, 0.0008 Å for *b*, 0.0004 Å for *c* and 0.02° for β

T [K]	*a* [Å]	*b* [Å]	*c* [Å]	β [°]
19	9.6195	8.6625	5.2630	109.93
100	9.6223	8.6638	5.2655	109.95
150	9.6269	8.6643	5.2691	109.97
170	9.6297	8.6644	5.2711	109.98
205	9.6356	8.6642	5.2758	110.01
225	9.6418	8.6634	5.2806	110.04
245	9.6542	8.6596	5.2886	110.11
265	9.6596	8.6598	5.2915	110.13
298	9.6641	8.6612	5.2924	110.12
373	9.6687	8.6639	5.2929	110.14
523	9.6784	8.6742	5.2953	110.10
723	9.6916	8.6906	5.2989	110.04
973	9.7095	8.7143	5.3042	109.96
1023	9.7132	8.7194	5.3054	109.95

Table 2 Crystal data and single-crystal structure refinement of Li-aegirine

	298 K	200 K	100 K
λ [Å]	0.71073	0.71073	0.71073
S.G.	*C*2/*c*	$P2_1/c$	$P2_1/c$
a [Å]	9.684(2)	9.635(2)	9.622(2)
b [Å]	8.661(2)	8.665(1)	8.664(1)
c [Å]	5.292(1)	5.275(1)	5.2555(9)
β [°]	110.12(3)	110.0(2)	109.95(2)
V [Å^3]	415.96	413.86	412.63
Z	4	4	4
Absorption coefficient	4.07	4.07	4.07
Index range	$-12 \le h \le 12$	$-13 \le h \le 13$	$-10 \le h \le 10$
	$-11 \le k \le 11$	$-12 \le k \le 12$	$-9 \le k \le 9$
	$-6 \le l \le 6$	$-7 \le l \le 7$	$-5 \le l \le 5$
Total meas. reflections	3173	5424	2399
Unique reflections	512	1239	638
R_{int}	0.0284	0.0298	0.0235
Refined parameters	47	77	72
GOF	1.140	1.068	1.027
$R_1[I > 4\sigma]$	0.0162	0.0227	0.0164
wR_2 [$I > 4\sigma$]	0.0483	0.0451	0.0447
R_1 all data	0.0198	0.0408	0.0241
wR_2 all data	0.0710	0.0661	0.0663
Largest diff. Paek/hole *e*/Å^3	0.44/−0.29	0.45/−0.43	0.33/−0.23

coordinates and equivalent isotropic displacement factors from single-crystal X-ray diffraction experiments can be found in Table 3 and bond length and bond angles for selected temperatures are given in Table 4. The room temperature structure of Li-aegirine (Fig. 2a) is consistent with the general *C*2/*c* clinopyroxene structure type (e.g., Clark et al. 1969; Cameron and Papike 1980). The Fe^{3+} (M1) cations are sixfold-coordinated and occupy the slightly distorted M1 octahedra, which are connected to each other by a common edge, forming zig-zag chains parallel to the *c*-axis. The Fe^{3+}–O interatomic distances range between 1.909(1) Å and 2.135(1) Å with $\langle Fe^{3+}–O\rangle = 2.024$ Å. The Li^+ (M2) cation is sixfold-coordinated and forms an irregular-shaped polyhedron, which is connected to three

Table 3 Atomic coordinates and equivalent isotropic displacement parameters [Å^2] for $LiFe^{3+}Si_2O_6$ at selected temperatures (E.S.D's in parantheses)

	x	*y*	*z*	U_{eq}
100 K				
Li	0.2504(4)	0.0090(4)	0.2367(5)	0.0009(6)
Fe	0.25022(3)	0.64788(3)	0.23528(5)	0.0006(1)
SiA	0.04779(7)	0.33899(6)	0.2776(1)	0.0007(1)
SiB	0.54862(6)	0.83874(6)	0.2527(1)	0.0007(1)
O(1A)	0.8673(2)	0.3327(2)	0.1636(3)	0.0023(3)
O(1B)	0.3674(2)	0.8347(2)	0.1351(3)	0.0022(3)
O(2A)	0.1160(2)	0.5086(2)	0.3123(3)	0.0032(4)
O(2B)	0.6215(2)	0.0032(2)	0.3537(3)	0.0033(3)
O(3A)	0.1085(2)	0.2667(2)	0.5821(3)	0.0030(3)
O(3B)	0.6050(2)	0.7232(2)	0.5120(2)	0.0028(4)
200 K				
Li	0.2505(6)	0.0097(4)	0.2395(8)	0.0072(6)
Fe	0.25020(4)	0.64794(6)	0.23841(6)	0.0013(1)
SiA	0.04739(7)	0.33888(7)	0.27481(9)	0.0013(1)
SiB	0.54760(7)	0.83922(7)	0.25575(9)	0.0011(1)
O(1A)	0.8668(2)	0.3331(2)	0.1602(3)	0.0025(3)
O(1B)	0.3668(2)	0.8350(2)	0.1384(3)	0.0027(3)
O(2A)	0.1158(2)	0.5087(2)	0.3145(3)	0.0047(3)
O(2B)	0.6199(2)	0.0052(2)	0.3473(3)	0.0044(3)
O(3A)	0.1080(2)	0.2637(2)	0.5775(3)	0.0042(3)
O(3B)	0.6049(2)	0.7298(2)	0.5219(3)	0.0045(3)
298 K				
Li	0	0.2624(5)	0.25	0.0106(8)
Fe	0	0.89832(3)	0.25	0.0029(1)
Si	0.29616(4)	0.08948(5)	0.26580(1)	0.0012(9)
O(1)	0.1159(1)	0.0848(1)	0.1496(2)	0.0057(2)
O(2)	0.3665(1)	0.2585(1)	0.3255(2)	0.0092(2)
O(3)	0.3557(1)	−0.0011(1)	0.0549(2)	0.0098(2)
1023 K (Rietveld refinement of X-ray powder data)				
Li	0	0.2841(29)	0.25	0.0240(7)
Fe	0	0.8955(5)	0.25	0.0021(5)
Si	0.2959(5)	0.0872(6)	0.2624(10)	0.0014(5)
O1	0.1166(9)	0.0875(10)	0.1481(10)	0.0027(1)
O2	0.3661(9)	0.2529(10)	0.3237(18)	0.0052(1)
O3	0.3567(9)	0.9986(10)	0.0474(22)	0.0036(1)

M1-octahedra by three common edges. The four shorter Li–O bond lengths [Li–O1 and Li–O2 with 2.076(4) Å and 2.180(4) Å, respectively] are those linking the M2 cation to the M1 chain, whereas the two Li–O3 interatomic distances [2.493(4) Å] cross-link the M2 cation to the basal plane of the tetrahedral chain. (Fig. 2a). The Li-cation exhibits large and anisotropic atomic displacement factors at room temperature with the principal mean square atomic displacement factors $\langle U^2\rangle$ being 0.0163, 0.0153, and 0.0093 Å^2. In contrast to the Ca- and Na-clinopyroxenes, where the M2 site is eightfold-coordinated, there is neither a common edge nor a common corner between the M2 polyhedra. In the Na- and Ca-clinopyroxenes, the M2 sites share a common edge with each other and also form a zig-zag chain parallel to *c*.

The silicate tetrahedra are linked by the bridging O3 oxygen atom. At room temperature (295 K) the tetrahedral chains are nearly fully expanded, expressed by an O3–O3–O3 angle of 180.83(7)°. In $LiFeSi_2O_6$ the SiO_4 tetrahedra exhibit a S-rotation (Thompson 1970). Within the Si^{4+} coordination sphere, the oxygens,

Table 4 Selected interatomic distances [Å] and bond angles [°] of synthetic Li-aegirine at selected temperatures [Atomic nomenclature after Burnham et al. (1967) for $C2/c$ and after Sato et al. (1995) for $P2_1/c$]

T [K] space group	1023[a] $C2/c$[b]	298 $C2/c$	230 $C2/c$	220 $P2_1/c$	200 $P2_1/c$	100 $P2_1/c$	
Fe–O1a1	2.032(8)[c]	2.029(1)	2.026(1)	2.026(2)	2.024(2)	2.024(1)	Fe–O1A
Fe–O1b1	2.032(8)	2.029(1)	2.026(1)	2.029(2)	2.028(2)	2.026(1)	Fe–O1B
Fe–O1a2	2.169(9)	2.135(1)	2.134(1)	2.132(2)	2.133(2)	2.130(2)	Fe–O1A
Fe–O1b2	2.169(9)	2.135(1)	2.134(1)	2.137(2)	2.139(2)	2.139(2)	Fe–O1B
Fe–O2c1	1.953(9)	1.909(1)	1.913(1)	1.910(2)	1.910(2)	1.910(2)	Fe–O2A
Fe–O2d1	1.953(9)	1.909(1)	1.913(1)	1.919(2)	1.920(2)	1.926(2)	Fe–O2B
⟨Fe–O⟩	2.051	2.024	2.024	2.025	2.026	2.026	⟨Fe–O⟩
Li–O1a1	2.229(20)	2.076(4)	2.068(4)	2.080(5)	2.076(5)	2.072(4)	Li–O1A
Li–O1b1	2.229(20)	2.076(4)	2.068(4)	2.065(5)	2.059(4)	2.060(4)	Li–O1B
Li–O2c2	2.183(10)	2.180(1)	2.172(2)	2.175(5)	2.178(4)	2.172(3)	Li–O2A
Li–O2d2	2.183(10)	2.180(1)	2.172(2)	2.132(5)	2.113(4)	2.090(3)	Li–O2B
Li–O3c1	2.420(18)	2.493(4)	2.499(4)	2.389(5)	2.380(5)	2.356(4)	Li–O3A
Li–O3d1	2.420(8)	2.493(4)	2.499(4)	2.681(4)[d]	2.724(4)[d]	2.796(4)[d]	Li–O3B
⟨Li–O⟩		2.201	2.196	2.168	2.161	2.150	⟨Li–O⟩
Si–O1	1.637(9)	1.636(1)	1.634(2)	1.637(2)	1.636(2)	1.634(2)	SiA–O1A
Si–O2	1.583(10)	1.599(1)	1.597(2)	1.596(2)	1.597(2)	1.594(2)	SiA–O2A
Si–O3a1	1.608(10)	1.623(1)	1.621(2)	1.620(2)	1.622(2)	1.628(2)	SiA–O3A
Si–O3a2	1.644(8)	1.629(1)	1.626(2)	1.636(2)	1.636(2)	1.632(2)	SiA–O3A
⟨Si–O⟩		1.622	1.620	1.622	1.623	1.622	⟨SiA–O⟩
O3–O3–O3	181.1(9)	180.83(7)	180.78(7)	189.01(8)	190.32(7)	192.55(7)	O3–O3–O3
				1.637(2)	1.638(2)	1.640(2)	SiB–O1B
				1.598(2)	1.599(2)	1.597(2)	SiB–O2B
				1.624(2)	1.626(2)	1.629(1)	SiB–O3B
				1.629(2)	1.628(2)	1.630(1)	SiB–O3B
				1.622	1.623	1.624	⟨SiB–O⟩
				167.76(7)	164.89(8)	160.02(7)	O3–O3–O3[a]

[a] Rietveld refinement of powder X-ray data
[b] In $C2/c$ the Si-positions are identical
[c] Standard deviations *in parentheses* refer to the last digit quoted
[d] Nonbonding Li–O interatomic distance in the $P2_1/c$ low temperature phase

forming the tetrahedral basal plane parallel to the b–c plane, exhibit strongly anisotropic displacements. This can be read off from the principal mean-squares atomic displacement parameters $\langle U^2 \rangle$ with 0.0190, 0.0077, and 0.0068 Å^2 for the bridging oxygen O3 and $\langle U^2 \rangle = 0.0142$, 0.0124, and 0.0060 Å^2 for O2. Compared to O2 and O3, the apical oxygen O1 is rather isotropic ($\langle U^2 \rangle = 0.0088$, 0.0077, and 0.0058 Å^2). The principal mean-squares atomic displacements of the oxygen decrease as temperature is lowered. These findings further underscore the instability of the tetrahedral chain with respect to kinking.

Upon cooling, first Bragg reflections (hkl) with $h + k \neq 2n$ (P reflections) appear at 230 K in the single crystal X-ray experiments; however, they are very weak in intensity. The C-centering of the cell is violated resulting in a primitive lattice below this temperature. At 230 K the structure can best be described in $C2/c$ as only the Bragg reflections (2 −3 −5) and (−7 0 4) have significant integrated intensity and violate the C-centering. Figure 3 shows the temperature-dependent variation of the integrated intensity of the Bragg reflections (2 −3 −5) and (−7 0 4) ($h + k \neq 2n$) and for comparison for the (−7 3 0) Bragg reflection ($h + k = 2n$). The P reflections gain rapidly in intensity in the 229 to 220 K region. Upon structure solution of the low-temperature form of $LiFe^{3+}Si_2O_6$, the space group $P2_1/c$, proposed by Behruzi et al. (1984), was confirmed. The most pronounced feature of the low-temperature structure of $LiFe^{3+}Si_2O_6$ is the presence of two nonequivalent Si^{4+} positions (SiA and SiB), giving rise to two tetrahedral chains with different rotation sense and tetrahedral kinking angles (S-rotation and 192.55(7)° for the A chain and O-rotation and 160.02(7)° for the B chain at 100 K, respectively). Figure 2 gives a comparison between the $C2/c$ and the $P2_1/c$ structure at 298 and 100 K, respectively. Corresponding to the two nonequivalent Si positions, six nonequivalent oxygen positions exist in the low-temperature form. The principal mean-square atomic displacements $\langle U^2 \rangle$ for the oxygens are rather isotropic (e.g., $\langle U^2 \rangle$ for O1A = 0.0035, 0.0030, and 0.0020 Å^2) in the $P2_1/c$ form. Plotting the tetrahedral kinking angle O3–O3–O3 as a function of temperature (Fig. 4) shows the most pronounced difference between the high- and low-temperature phase. Upon cooling, the O3–O3–O3 angle slightly decreases to 180.78(8)° in the $C2/c$ phase at 230 K. Further cooling yields the $C2/c \rightarrow P2_1/c$ phase transition. At temperatures just below the phase transition, the two nonequivalent tetrahedral chains in the $P2_1/c$ phase show nearly identical rotations from 180°, e.g., 5.88(8)° at 227 K, corresponding to O3–O3–O3 angles of 185.88(7)° in the A-chain and 174.12(8)° in the B-chain. The difference in the tetrahedral kinking angle increases as the temperature is lowered further, with the SiB chain be-

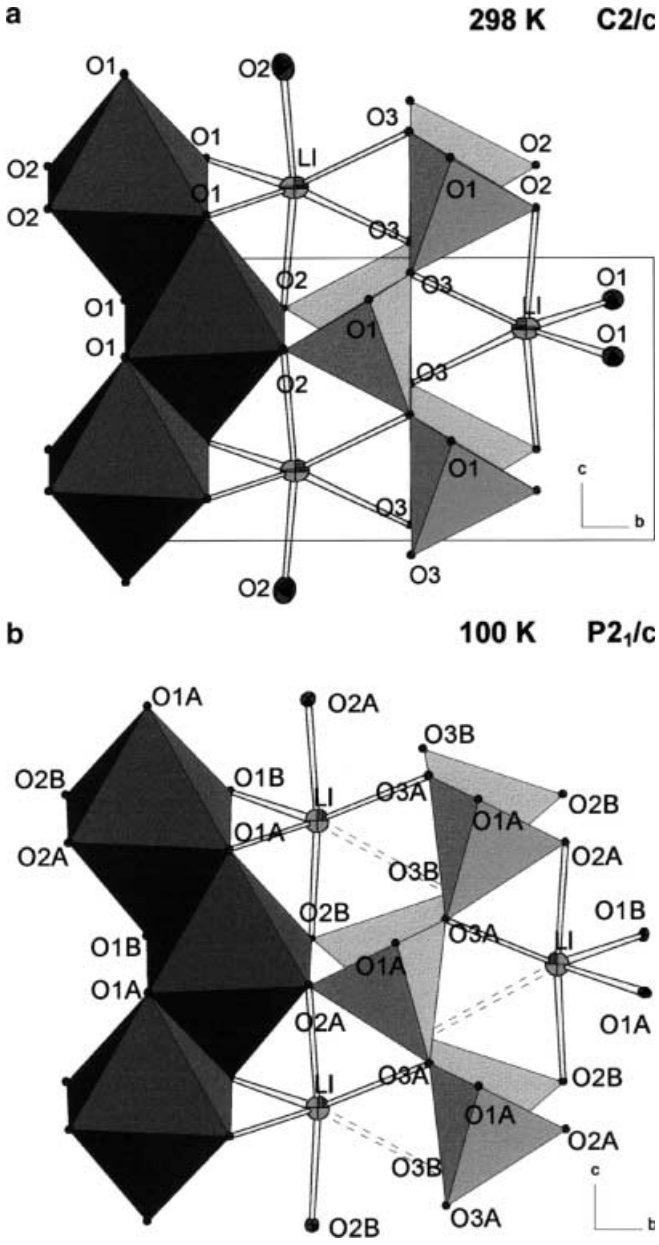

Fig. 2a, b Comparison of the $C2/c$ high-temperature structure of $LiFe^{3+}Si_2O_6$ at 298 K with the $P2_1/c$ low-temperature structure at 100 K, as determined from single-crystal X-ray diffraction experiments and viewed along the crystallographic a-axis. In the $P2_1/c$ phase, the Li–O3B bond length (*dashed bond*) moves out of the Li-coordination sphere. The atomic nomenclature for the $C2/c$ high-temperature phase after Burnham et al. (1967) and for the $P2_1/c$ low-temperature phase after Sato et al. (1995) is displayed

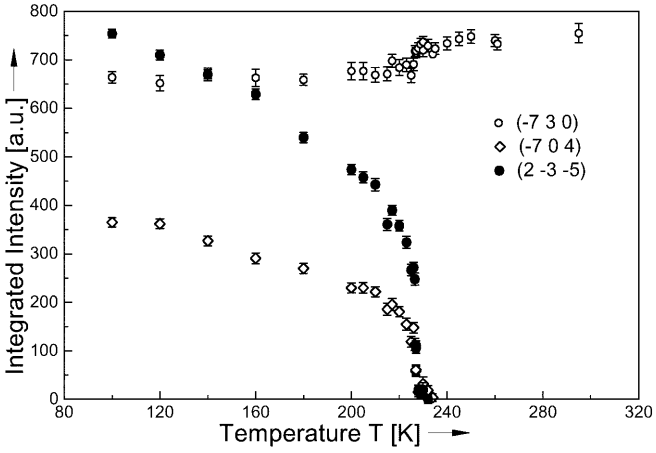

Fig. 3 Temperature-dependent variation the integrated intensity of the Bragg reflections (2 −3 −5) and (−7 0 4), ($h + k \neq 2n$, P-reflection), and for comparison for the (−7 3 0) Bragg-reflection, ($h + k = 2n$) for $LiFe^{3+}Si_2O_6$ from single-crystal X-ray diffraction experiments. The P-reflections rapidly gain intensity in the 230–220 K region

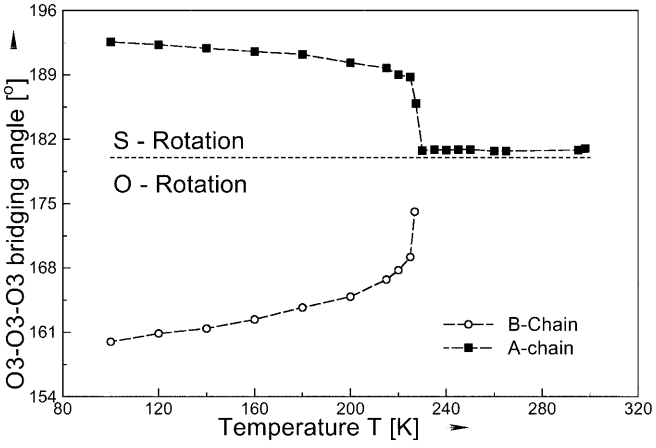

Fig. 4 Temperature-dependent variation of the tetrahedral kinking angle O3–O3–O3 in $LiFe^{3+}Si_2O_6$ as determined from single-crystal X-ray diffraction experiments

coming more kinked than the SiA chain. At 100 K the difference in kinking angle amounts to ≈8°. The interatomic distances for the SiA and the SiB tetrahedron are very similar, the SiB tetrahedron is slightly larger. Furthermore, the temperature variation in the Si–O bond lengths is very small.

Upon cooling, the most pronounced changes in the Li-coordination sphere are connected with the two nonequivalent O3 oxygens (Fig. 5a). The coordination of Li^+ decreases from six to five upon the $C2/c \rightarrow P2_1/c$ phase transition. As a consequence of the increased kinking of the tetrahedral chains, the O3A oxygen is moved closer to the Li^+ cation [2.356(4) Å at 100 K] as compared to 2.499(4) Å at 230 K ($C2/c$ phase), whereas the O3B oxygen is continuously moved further away from the Li^+ cation. At 100 K, the Li–O3B interatomic distance is 2.796(4) Å. Li–O3 bond length, as extracted from Rietveld refinements of powder X-ray data, for temperatures $T > 300$ K are included to show the high-temperature behavior. They follow the same trend as found for the single-crystal data between 230 and 300 K. There are also pronounced changes in the Li–O2A and Li–O2B bond lengths (Fig. 5b). While the slope of the decrease of the Li–O2A interatomic distance is very similar for temperatures above and below 300 K, the Li–O2B bond length becomes significantly shortened at temperatures $T < 230$ K, i.e. below the phase transi-

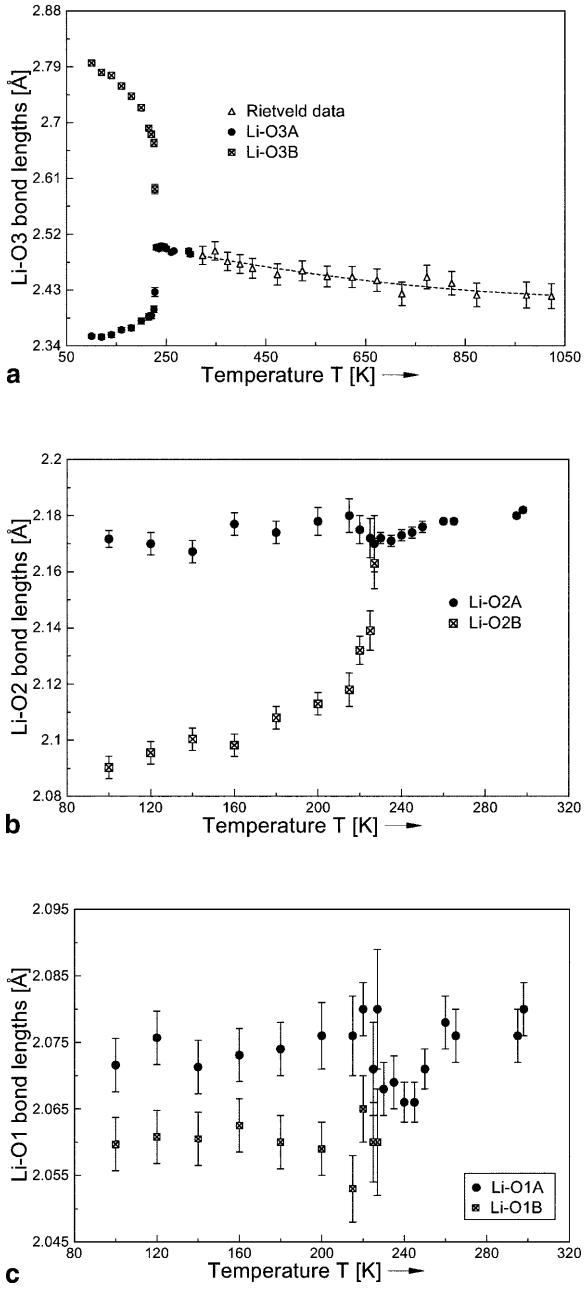

Fig. 5a–c Variation of individual Li–O bond lengths of $LiFe^{3+}Si_2O_6$ as a function of temperature as determined from single-crystal X-ray diffraction experiments. Li–O3 bond lengths in **a** for the high-temperature region ($T > 300$ K) are from Rietveld refinements of X-ray powder diffraction experiments

tion, as a consequence of tetrahedral B-chain rotation. For temperatures $T > 300$ K the Li–O2 distance increases linearly up to 2.23(2) Å at 1023 K. Only small changes occur for the Li–O1 bond length (Fig. 5c). The LiO1A and LiO1B interatomic distances are rather similar. Upon heating, the Li–O1 interatomic distance increases linearly up to 2.18(1) Å at 1023 K.

Figure 6 displays the changes in Fe^{3+}–O interatomic distances as a function of temperature between 100 and 300 K. The two shorter Fe^{3+}–O1 distances show only little variation with temperature and the differences between Fe–O1A and Fe–O1B in the low-temperature phase are very small (Fig. 6a). Increasing temperature up to 1023 K does not increase the short Fe–O1 bond. The two larger Fe–O1 bonds (Fig. 6b) also are rather similar in the low-temperature form with the larger Fe–O1A bond becoming larger with increasing temperature, whereas the larger Fe–O1B bonds remains rather constant. It is interesting to note that the two larger Fe–O1 bonds become slightly shortened with increasing temperature above the phase transition temperature. However, this trend is reversed above ≈ 300 K, as indicated by the high-temperature Rietveld data (Fig. 6c). Between 323 and 1023 K, the larger Fe–O1 bond increases by 1.8%. Similar observations can be made for the Fe–O2 bonds (Fig. 6d).

Magnetic structure

As already outlined in Lottermoser et al. (1998), first occurrence of magnetic reflections can be observed in the powder neutron scattering pattern at 17.5 K. A significant increase in the background between 10° and 20° 2Θ ($\lambda = 2.4249$ Å) is already observed at temperatures $T < 30$ K. The two first and strong magnetic reflections in the diffraction pattern at 15.30° and 16.04° 2Θ at 1.4 K were indexed as $(100)_m$ and $(010)_m$, respectively. Single-crystal SQUID magnetic measurements by Baum et al. (1988) showed no magnetic moments being aligned along the *b*-axis. This was confirmed by our neutron diffraction measurements. The Rietveld refinement of the magnetic phase below 16 K reveals the magnetic moments to be aligned in the *a*–*c* plane with the main component of the magnetic moment along the crystallographic *c*-axis (4.88 μ_B at 1.4 K) and a small component of 0.8 μ_B (1.4 K) aligned along the *a*-axis. The resulting magnetic moment amounts to $\mathbf{m}_o = 4.93\ \mu_B$ with an angle of 8.3° between the moment vector $\mathbf{m}_o$ and the *c*-axis at 1.4 K. Figure 7 shows the evolution of the components of the magnetic moment along the crystallographic axes *a* and *c* as a function of temperature. The angle between the moment vector $\mathbf{m}_o$ and the *c*-axis changes with temperature. We propose the Shubnikov group $P2_1/c$ as being the magnetic space group for $LiFe^{3+}Si_2O_6$. This is in accordance with the antiferromagnetic ordering within and between the $Fe^{3+}O_6$ chains in agreement with the findings of magnetic measurements. Figure 8 combines the integrated intensities of the strong magnetic Bragg reflections $(100)_m$ and $(010)_m$, as extracted from the neutron diffraction experiments, with the results of SQUID magnetic measurements as a function of temperature at an external field of 1 Tesla. The molar magnetic susceptibility of $LiFe^{3+}Si_2O_6$ shows a maximum at 20.8 K and an inflection point at 17.5 K. The latter temperature is in close agreement with the first appearance of magnetic reflections in the neutron scattering experiments. From Curie-Weiss behavior of the inverse magnetic suscepti-

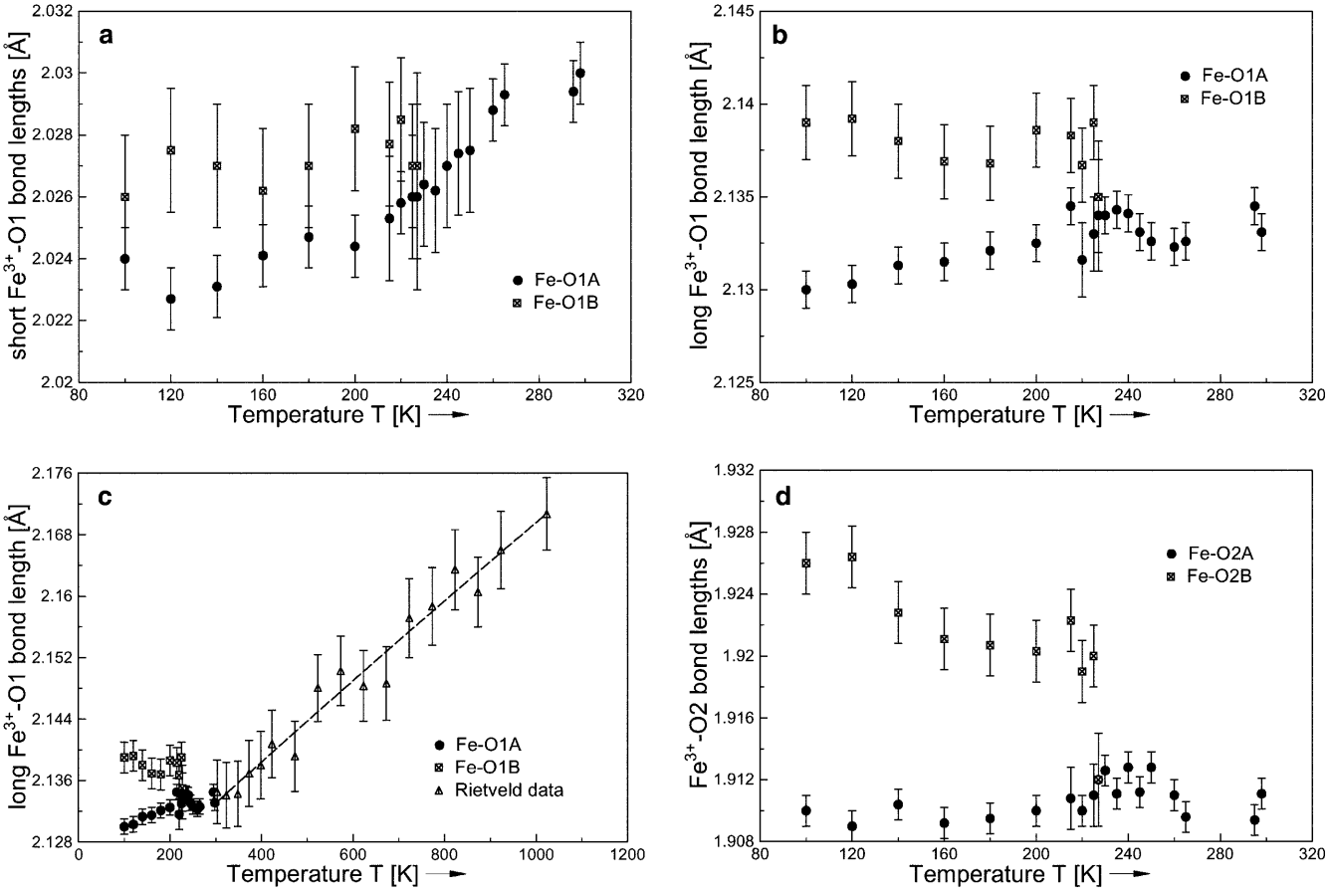

Fig. 6a–d Variation of individual Fe^{3+}–O bond lengths of $LiFe^{3+}Si_2O_6$ as a function of temperature as determined from single-crystal X-ray diffraction experiments. Data in **c** for temperatures $T > 300$ K are from Rietveld refinements of X-ray powder diffraction experiments

bility above 100 K, an experimental magnetic moment $\mu_{CW} = 5.81\ \mu_B$ and a paramagnetic Curie temperature $\Theta_P = -25.8$ K was extracted.

Mössbauer spectroscopy

^{57}Fe transmission Mössbauer spectra on the identical powder sample of $LiFe^{3+}Si_2O_6$, which was also used for the powder neutron diffraction experiments, were recorded between 80 and 450 K. The ^{57}Fe Mössbauer spectrum consists of two symmetric and narrow split resonance absorption lines corresponding to one Lorentzian-shaped doublet for Fe^{3+} on the M1 position. No sign for Fe^{2+} could be detected. The most striking result of the Mössbauer spectroscopic investigations is shown in Fig. 9. Within the temperature variation of the ferric quadrupole splitting Δ we observed a discontinuity in the temperature range between 200 and 250 K. Above 260 K the typical small increase in Δ with increasing temperature is observable. The same applies for temperatures $T < 200$ K. Within the range of the dramatic decrease of Δ Fe^{3+} we observe two different slopes with

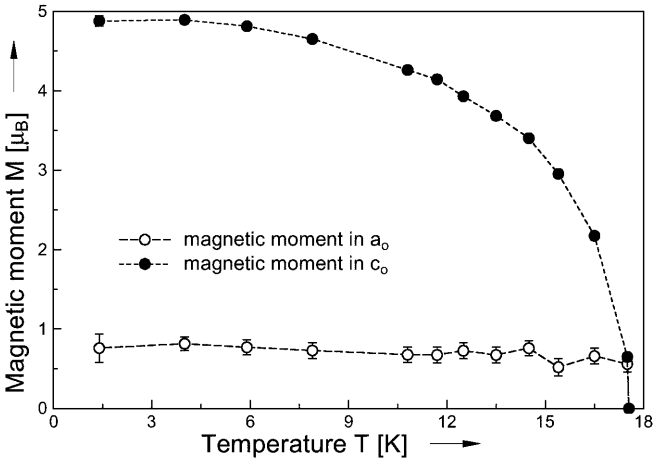

Fig. 7 Evolution of the components of the magnetic moment [μ_B] along the crystallographic axes *a* and *c* as a function of temperature as determined from Rietveld refinements of powder neutron diffraction data ($\lambda = 2.4148$ Å)

a kink at the $P2_1/c \rightarrow C2/c$ phase transition. This drop of ferric quadrupole splitting seems to be supported by single-crystal measurements on $LiFe^{3+}Si_2O_6$ (Lottermoser et al. 1998) with the **k**-vector of the incident γ-ray parallel to *b* between room temperature and 25 K. The characteristic orientation angle β between the main component of the electric field gradient V_{zz} and the crystallographic *b*-axis remains constant at 42° between

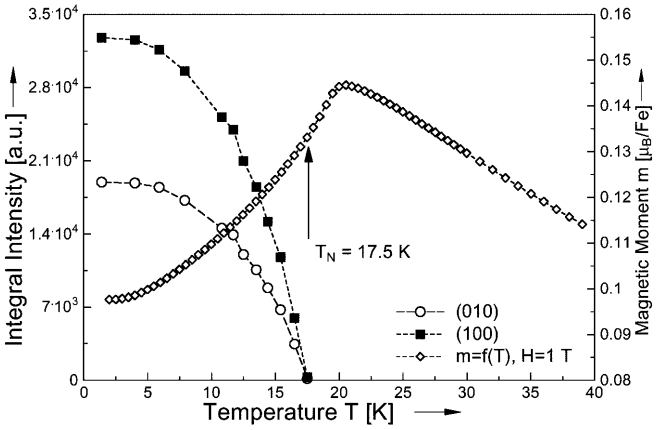

Fig. 8 Evolution of the integrated intensity of the strong magnetic Bragg reflections $(100)_m$ and $(010)_m$ of $LiFe^{3+}Si_2O_6$ from neutron powder diffraction experiments ($\lambda = 2.4148$ Å) as a function of temperature, combined with the molar magnetic susceptibility, measured at an external field of 1 Tesla

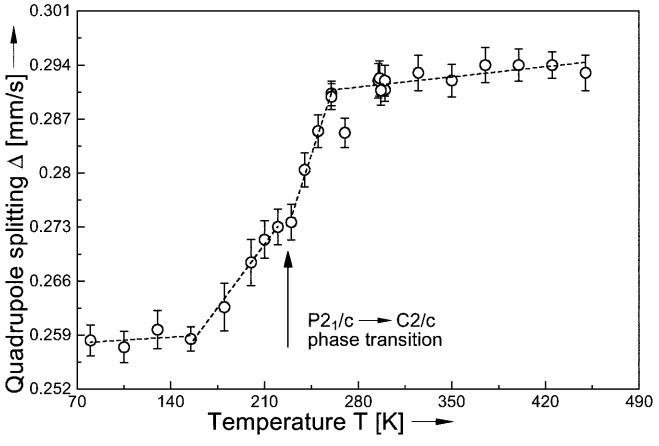

Fig. 9 Variation of the quadrupole splitting Δ of Fe^{3+} in $LiFe^{3+}Si_2O_6$ as a function of temperature

300 and 210 K [$\beta = 41.9(6)°$, 42.2(5)°, and 42.1(6)° at 300, 240, and 210 K, respectively]. Below this temperature we observe an increase of β to $\approx 44°$ down to low temperatures [$\beta = 43.7(6)°$, 44.4(1.1)°, 43.4(0.7)°, and 46.7(5)° at 180, 25, 15, and 10 K, respectively).

Discussion and conclusion

The $C2/c \rightarrow P2_1/c$ phase transition in $LiFe^{3+}Si_2O_6$, proposed by Behruzi et al. (1984), was fully confirmed and thoroughly investigated. We found a transition temperature of 230 K, in close agreement with the one found by Behruzi et al. (1984) from DTA measurements.

We assume the driving force for the $C \rightarrow P$ transition in $LiFe^{3+}Si_2O_6$ to be an instability with respect to a kinking of the SiO_4 tetrahedral chains, which are nearly fully extended just above the phase transition. The large anisotropic vibration of the bridging O3 oxygen perpendicular to the Si–O–Si direction in the *C*-phase above the phase transition is interpreted as a precursor effect with a beginning distortion of the *C*-centered structure. During the phase transition the tetrahedral chains become kinked by more than 10° within a few Kelvin. Another peculiarity is the appearance of two differently distorted tetrahedral chains in the low-temperature phase. It is tempting to speculate about the reason for this behavior. The different thermal expansion of the tetrahedral and the octahedral site may play a role in inducing the phase transition. The SiO_4 tetrahedra remain very rigid in size upon cooling whereas the $Fe^{3+}O_6$ octahedra decrease in size. Upon cooling, matching of the two units, cross-linked to each other via the O2 oxygens, can be achieved by variation of the tetrahedral chain-bridging angle within the $C2/c$ phase. However, this will not work for the fully extended tetrahedral chains of $LiFe^{3+}Si_2O_6$ with the bridging angle of $\approx 181°$ at temperatures close to 300 K.

$LiFe^{3+}Si_2O_6$ therefore has to find another way of accommodating to the proposed mismatch. The increase in the larger Fe^{3+}–O1 and the Fe^{3+}–O2 bonds with decreasing temperature between 300 and 230 K is assigned to the attempt to match octahedral and tetrahedral chain to each other. This holds true especially for the Fe^{3+}–O2 bonds, as O2 is the connection point between these two building units. The shorter bonds between Fe^{3+} and the O1 oxygens, which cross-link the Li-polyhedron to the octahedral chain, are not affected by this proposed structural misfit, and decrease in length with decreasing temperature, as expected. They remain rather unaffected by the changes within the 230–300 K region described above. Obviously, increasing the longer Fe^{3+}–O1 and the Fe–O2 bond lengths will not work at temperatures lower than 230 K. This results in a decrease in symmetry from *C* to *P*, where two nonequivalent tetrahedral chains are now possible. This facilitates different kinking angles of the two tetrahedral chains and higher flexibility in adjusting the tetrahedral to the octahedral chains as temperature is lowered further.

Mechanisms other than sole geometric structural misfits between the octahedral and tetrahedral chains also have to be considered. Kanoite $MnMgSi_2O_6$ exhibits an O3–O3–O3 angle as low as 175.4(2)° about 20 K above the $P2_1/c \rightarrow C2/c$ phase transition at 500–520 K (Arlt and Armbruster 1997). Some influence seems to be exerted by the kind of M2 and M1 cations. Arlt and Armbruster (1997) report the $P2_1/c \rightarrow C2/c$ phase transition in kanoite to be shifted to higher temperatures as Ca^{2+} enters the M2 site. More detailed investigations on different clinopyroxenes with variable chemical compositions must be made to find out additional criteria suitable to predict the presence and temperature of the displacive $C2/c \rightarrow P2_1/c$ phase transition.

The M2 sites in $LiFe^{3+}Si_2O_6$ do not form a zig-zag chain as found in other $C2/c$ clinopyroxenes. The Li-site is highly distorted, with four shorter and two longer

bonds. Within the Li-coordination sphere distinct changes were observed as a function of temperature. While the Li–O1 and Li–O2 bonds are positively correlated with temperature in the $C2/c$ phase, the Li–O3 bond increases with decreasing temperature. This is solely due to the increase in tetrahedral chain stretching with decreasing temperature. During the phase transition, the coordination of Li decreases from six to five and becomes slightly more regular, with four shorter and one longer bond. The coordination to the O3B oxygen is lost. No pronounced discontinuities are present for the Li–O1 bonds during phase transition.

There is a pronounced shrinking of the lattice in the c direction upon cooling in the 240 to 200 K region. This can easily be ascribed to the kinking of the tetrahedral chains aligned parallel to the c-axis. This kinking of tetrahedral chains during the phase transition induces a small increase in b and also a contraction of the octahedral layer parallel to a. Arlt and Armbruster (1997) observed similar trends during the $P2_1/c \rightarrow C2/c$ phase transition in kanoite.

The low-temperature contraction of the lattice is consistent with the magnetic phase transition. The most pronounced magneto-striction of the lattice is observed within the b–c plane, only weak magneto-striction is found parallel to a. This goes along with the findings that the magnetic moments are mainly aligned parallel to c with a small angle towards a. The decrease in b and in the monoclinic angle β reflects the antiferromagnetic coupling between neighboring Fe^{3+} chains.

^{57}Fe Mössbauer spectroscopic data also reflect the $C \rightarrow P$ phase transition, especially the ferric iron quadrupole splitting. As ferric iron possesses a symmetric electron configuration ($3d^5$ ion), the quadrupole splitting of Fe^{3+} is dominated by the lattice term contribution to the electric field gradient. The observed decrease in ferric quadrupole splitting in the 180–260-K range can be directly ascribed to altered geometric environments around the probe nucleus ^{57}Fe due to the $C2/c \rightarrow P2_1/c$ phase transition. The decrease in ferric quadrupole splitting suggests a decrease in polyhedral distortion for the $Fe^{3+}O_6$ octahedron in the $P2_1/c$ phase. This is exactly what is being observed in the bond-length distortion parameters for the M1 site. The phase transition at 228 K should also be observable as a change in the orientation of the electric field gradient. In fact, there are slight reorientations expressed by a change of the angle between the b axis and V_{zz} (Lottermoser et al. 1998). Once again, Mössbauer spectroscopy has proven to be very sensitive to even small changes in the local geometric environment around the Fe probe nucleus, accompanying the $C2/c \rightarrow P2_1/c$ phase transition in $LiFe^{3+}Si_2O_6$.

Acknowledgements G.J.R. wishes to thank the Alexander von Humboldt-Stiftung for the 18 months' support in 1998–1999 through a Humboldt research fellowship. The financial support to G.J.R. by the Fonds zur Förderung der wissenschaftlichen Forschung (Austria) through an Erwin-Schrödinger-Stipendium, grant no J1810-GEO, is greatly acknowledged. We are grateful to J. Ernst (Aachen) for his kind help with the high-pressure synthesis experiments.

References

Arlt T, Armbruster Th (1997) The temperature-dependent $P2_1/c$–$C2/c$ phase transition in the clinopyroxene kanoite $MnMg[Si_2O_6]$: a single-crystal X-ray and optical study. Eur J Mineral 9: 953–964

Baum E, Treutmann W, Behruzi M, Lottermoser W, Amthauer G (1988) Structural and magnetic properties of the clinopyroxenes $NaFeSi_2O_6$ and $LiFeSi_2O_6$. Z Kristallogr 183: 273–284

Behruzi M, Hahn T, Prewitt CT, Baldwin K (1984) Low- and high-temperature crystal structures of $LiFeGe_2O_6$, $LiFeSi_2O_6$ and $LiCrSi_2O_6$. Acta Crystallogr (A)40 Suppl C-247

Burnham CW, Clark JR, Papike JJ (1967) A proposed nomenclature for clinoyroxene structure. Z Kristallogr 125: 109–119

Cagliotti G, Paoletti A, Ricci FP (1958) Choice of collimators for a crystal spectrometer fro neutron diffraction. Nucl Instr 3: 223–228

Cameron M, Papike JJ (1980) Crystal chemistry of silicate pyroxenes. In: Prewitt CT (ed) Pyroxenes. Mineral Soc Am, Reviews in Mineralogy 7: 5–91

Clark JR, Appleman DE, Papike JJ (1969) Crystal chemical characterisation of clinopyroxenes based on eight new crystal structure refinements. Min Soc Am Spec Pap 2: 31–50

Lottermoser W, Redhammer G, Forcher K, Amthauer G, Paulus W, Andre G, Treutmann W (1998) Single-crystal Mössbauer and neutron powder diffraction measurements on the synthetic clinopyroxene Li-acmite $LiFeSi_2O_6$. Z Kristallogr 213: 101–107

Rietveld HM (1969) A profile refinement method for nuclear and magnetic structures. J Appl Crystallogr 2: 65–71

Rodrigues-Carvajal J (1996) FULLPROF; Rietveld, profile matching and integrated intensity refinement of X-ray and/or neutron data (PC version). Version 1.3c (1996)

Sato A, Osawa T, Ohashi H (1995) Low-temperature form of $LiGaSi_2O_6$. Acta Crystallogr (C) 51: 1959–1960

Sheldrick G (1993) SHELXL, a program for refining crystal structures. University Göttingen, Germany

Stoe & Cie (1996) X-SHAPE and X-RED: programs for optimization of the crystal shape (w.r.t. the merging R-value) and numerical absorption correction, Stoe & Cie

Thompson JB Jr (1970) Geometric possibilities of amphibole structures: model biopyriboles. Am Mineral 55: 292–293